RSCPublishing | Journal of Materials Chemistry B

Preparation of soft and interconnected macroporous hydroxypropylcellulose methacrylate scaffold for adipose tissue engineering

Journal:	*Journal of Materials Chemistry B*
Manuscript ID:	TB-ART-11-2012-000446.R2
Article Type:	Paper
Date Submitted by the Author:	n/a
Complete List of Authors:	Hoo, Siew Pei; RMIT University, Chemistry Loh, Qiu Li; Nanyang Technological University, School of Materials Science & Engineering Yue, Zhilian; RMIT University, Chemistry Fu, Jing; Monash University, Department of Mechanical & Aerospace Engineering Tan, Timothy Thatt Yang; Nanyang Technological University , School of Chemical and Biomedical Engineering Choong, Cleo; Nanyang Technological University, Materials Science Chan, Peggy; RMIT University,

SCHOLARONE™
Manuscripts

Journal of Materials Chemistry

Dynamic Article Links ▶

PAPER

Preparation of soft and interconnected macroporous hydroxypropylcellulose methacrylate scaffold for adipose tissue engineering

Siew Pei Hoo[a,b,c], Qiu Li Loh[d], Zhilian Yue[e], Jing Fu[f], Timothy T.Y.Tan[g], Cleo Choong*[d], Peggy P.Y.
5 **Chan*[b,c]**

This study describes the preparation and characterization of a biodegradable 3D hydrogel constructed from hydroxypropyl cellulose (HPC), modified with bifunctional methacrylic anhydride (MA) to form
10 hydroxpropyl cellulose methacrylate (HPC-MA), for adipose tissue engineering applications. The hydrogels were prepared from three different concentrations (10 wt%, 15 wt% and 20 wt%) of HPC-MA with 0.35 degree of substitution. HPC-MA hydrogel scaffolds with open biphasic feature were prepared by exploiting the thermal responsive phase behavior of HPC and temperature mediated phase separation of HPC-MA. The resulting scaffolds exhibited pore size ranging from 30 to 300 μm and interconnected
15 porosity of ~90 %. The swelling ratio (SR) and storage modulus of HPC-MA scaffolds were in the range of 12.94 - to 35.83 and 0.75 - to 4.28 kPa, respectively. The swelling ratio and storage modulus suggested that the scaffold exhibits high water retention, allowing medium exchange during cell culturing and suitable for adipose tissues regeneration. The HPC-MA scaffolds were found to be biocompatible to human adipose-derived stem cells (ASCs). ASCs were successfully differentiated into the adipocytes
20 inside the scaffolds, and therefore demonstrated the potential application of these HPC-MA scaffolds for adipose tissue engineering.

Introduction

Currently, there is a need for transplantable and functional adipose tissue to restore lost or damaged tissue due to post-
25 traumatic loss, lipoatrophy, tumor removal or congenital defects[1-3]. A scaffold-based tissue engineering approach is a promising alternative to current autologous fat grafts as it addresses the issue of donor site morbidity as well as other complications associated with fat graft transfers including fat necrosis and
30 volume reduction over time[4]. In general, an ideal scaffold for adipose tissue application should: (1) be constructed from materials with controlled biodegradability or bioresorbability so that new adipose tissues will eventually replace the scaffold, (2) possess an extensive network of interconnecting pores to promote
35 nutrient and waste exchange, (3) provide appropriate surface chemistry to facilitate cellular attachment, differentiation and proliferation, (4) be easily fabricated into a variety of shapes and sizes, (5) mimics the soft and elastic texture of native tissues, and (6) provides appropriate mechanical strength that can withstand
40 post-implantation forces exerted on the tissue[5-7]. The mechanical properties of the scaffold are of particular importance as mechanical stimuli has been shown to regulate the differentiation response of seeded stem cells[8]. Ideally, the scaffolding material

should mimic the property of the tissue it is replacing, and in the
45 case of adipose tissue, a Young moduli range of 3-4 kPa has been reported[9, 10].

Cell-based tissue engineering using scaffolds offers great promise for repair of adipose tissue. Human adipose-derived stem cells (ASCs) are multipotent mesenchymal stem cells derived
50 from the stromal vascular fraction of adipose tissue, and are available abundantly as they can be isolated from adipose tissue by liposuction or abdominoplasty[1, 11, 12]. ASCs are capable of differentiating into a variety of mesenchymal lineages including mature adipocytes[9, 13, 14]. ASCs have also been shown to secrete
55 factors that trigger host stem cell migration to the implantation site, thus contributing to tissue regeneration. Increasing evidence suggested that increases in adipose tissue are associated with increases in microcirculation[2]. ASCs have also been shown to modulate immune response and have the potential to avoid tissue
60 rejection[9]. ASCs are therefore an attractive cell source for adipose tissue engineering and regenerative therapeutic applications.

The use of 3-dimensional (3D) scaffold as ASCs culturing system is considered to be advantageous compared to 2-dimensional (2D) monolayer culture, since 3D systems can closely mimic the
65 microenvironment that cells experience in vivo[15] Girandon et al., has demonstrated that ASC cultured in 3D scaffold expressed

higher level of specific adipogenic markers as compared to 2D culture[16]. A literature review by Flynn & Woodhouse[17] has summarized the results from studies that investigate the use of a range of synthetic and naturally derived scaffolds for adipose tissue engineering. Although a number of scaffolds have shown to facilitate adipose tissue regeneration, new biomaterials are still required to provide multifunctional platforms that incorporate biochemical and physiochemical properties that can be beneficial to adipose tissue engineering.

Scaffold pore sizes, porosity and pore interconnectivity are critical parameters that influence cell binding, migration, intracellular signalling, vascularization, ECM production, cell phenotype, nutrient transport, gas diffusion, and metabolic waste removal, thus determining scaffold performance. The pore size of the 3D scaffold must be large enough to accommodate increase in cell number and increase in volume associated with lipid formation[5] and for cells to migrate through the pores, but the pore size should also be small enough to retain a critical total surface area for appropriate cell binding[18, 19]. There has not been extensive research on the optimum pore size for human adipose-derived stem cells. However, in general, the accepted optimum pore size of tissue scaffold for the majority of mammalian cells such as liver tissue regeneration, fibroblast ingrowth and bladder smooth muscle cell attachment and ingrowth should be within the range of 38 to 500 μm, and the optimum porosity should be above 90 %[18-23]. A variety of techniques have been developed to fabricate porous structure including solvent casting, gas forming, solvent-casting and porogen leaching, solvent induced phase separation, electrospinning, emulsion freeze drying, fiber bonding, or a mixture of these techniques. Although these techniques can produce highly porous scaffold, these methods have limited control over scaffold architecture, pore interconnectivity, poor strength and in some instances require the use of toxic solvent[20-22]. For example, solvent-casting and porogen leaching method produces porous structure with controllable pore size and porosity, however the resulting scaffolds often exhibit porous structure with closed pore walls, thus impeding nutrient transport and cell infiltration within the scaffold[24].

There is a growing awareness of developing biomaterials using renewable resources such as cellulosic materials[25, 26]. Hydroxypropylcellulose (HPC) is a commercial derivative of cellulose and Food and Drug Administration (FDA)-approved agent for drug delivery applications. HPC is available abundantly at low cost, soluble in water as well as in a variety of organic solvents, commercially available in a range of molecular weights, making it an attractive biomaterial. More importantly, HPC exhibits phase transition from isotropic aqueous solution to meta-stable biphasic system above its lower critical solution temperature[26, 27]. In a previous study[26], hydroxypropyl cellulose (HPC) was modified with allyl isocyanate containing urethane group and fabricated into a 3D interconnected porous scaffold by immobilizing biphasic HPC via gamma-ray irradiated crosslinking. This method produced biocompatible scaffolds with interconnected macroporous structure with porosity of approximately 90 %. Despite the advantages of allyl isocyanate modified HPC, it is not biodegradable due to the lack of cellulose hydrolyses in vivo. In addition, polymers with repeating unit that contains urethane moiety are generally regarded to have limited biodegradability. For example, polyurethanes are typically used as non-biodegradable coatings. Synthesis of biodegradable polyurethane requires the polyurethane to be produced from diisocyanate precursor such as lysine-dissocyanaate that release nontoxic degradation products such as lysine[28].

Herein, we prepare biodegradable and macroporous scaffold structures taking advantages of the temperature responsive property of HPC. HPC was first modified with a bifunctional methacrylic anhydride (MA). The resulting conjugate contains photo-crosslinkable and hydrolytically degradable methacrylate pendant group. The modified HPC conjugates, namely HPC-MA, were polymerized at its colloidal state induced by temperature mediated phase separation, thereby immobilizing the biphasic feature of HPC. The phase separation was induced in aqueous solvent simply by warming an aqueous solution containing HPC-MA to above 40°C, and avoids the use of organic solvent and thus the problem associated with harmful organic solvent residue. The physiochemical properties such as swelling ratio, porosity, mechanical properties and interior morphologies of these HPC-MA scaffolds were evaluated. Cytotoxicity studies using human adipose-derived stem cells (ASCs) were carried out to examine the biocompatibility of the scaffold. The current novel HPC-MA scaffold was then investigated as a support for the proliferation and adipogenesis of ASCs.

Experimental

Synthesis scheme and ^{1}H nuclear magnetic resonance (NMR)

Hydroxypropyl cellulose (HPC, M_n 10, 000 g/mol, Sigma-Aldrich) was dehydrated by azeotropic distillation at 50 °C in toluene to remove the moisture before use. The HPC hydrogel precursor, namely HPC-MA conjugate, was prepared by modifying cellulose with methacrylic anhydride (MA). Briefly, 4.0 g of dehydrated HPC was dissolved in 150 mL of chloroform followed by 4.17 mmole of methacrylic anhydride (MA). 4.17 mmole of N'N-dicyclohexylcardodiimide (DCC) was first dissolved in 3 mL of chloroform before adding dropwise in the HPC chloroform mixture. The solution was stirred for 48 h in the presence of 0.4 g of 4-dimethylaminopyrinde (DMAP) as catalyst. The product was concentrated and precipitated into diethyl ether. Further purification was carried out by repeating dissolution in chloroform and precipitation into diethyl ether. Finally, the product was dissolved in water, filtered, and dialyzed against deionised water for 72 h before lyophilisation in a freeze dryer (HETO PowerDry PL6000, Thermo Scientific). The ^{1}H NMR spectra of lyophilised HPC-MA sample were obtained in deuterated chloroform (CDCl$_3$) using a NMR operating at 300MHz (Bruker, ACF 300).

Preparation of HPC scaffolds and turbidity

The turbidity of HPC-MA conjugate was measured to determine its lower critical solution temperature. A 10 %w/v HPC-MA aqueous solution was selected as an indication of the LCST. In brief, the lyophilised HPC-MA was dissolved in deionised water. The transmittance of the sample was monitored as a function of temperature at a fixed wavelength of 500 nm, using a UV/Vis

spectrophotometer (Agilent Technologies Cary 60 UV-VIS, Australia) with the sample cell thermostated by a temperature controller with circulating water bath. The transmittance was measured four times and the average transmittance values of the
5 measurement were reported

Lyophilisation HPC-MA conjugate was dissolved in deionised water (10 %, 15 % and 20 % w/v respectively), followed by adding 3-5 % final concentration of 2-hydroxy-1-[4-(2-hydroxyethoxy)phenyl]-2-methyl-1-propanone, known as
10 Irgacure 2959, (Sigma-Aldrich) as photoinitiator. The solution was placed in a water bath at 45 °C for 10 minutes to induce phase separation. The emulsion solution was then crosslinked in a ultra-violet ray (UV) crosslinker (Honle UV Technology, UV-F 400) for approximately 6 minutes. The crosslinked gels were then
15 washed with deionised water to remove any un-crosslinked HPC-MA conjugate and photoinitiator before lyophilisation. HPC scaffold, after reaching their maximum swollen state in water in room temperature, were frozen at -20 °C freezer and lyophilised under vacuum for 48 h until all water was sublimed. The
20 scaffolds prepared from 10 %, 15 %, and 20% (w/v) of HPC-MA were denoted as HPC-MA-10%, HPC-MA-15%, and HPC-MA-20%, respectively.

Swelling ratio and Mechanical properties

25 Swelling ratio of the scaffold was measured using a conventional gravimetrically method. The lyophilised HPC scaffolds with different polymer concentrations were submerged in water at room temperature for 48 h. The weight of the swollen sample was obtained after wiping off excess water on the surface with a moist
30 filter paper and the dry weight of the sample was measured after drying the sample under vacuum at 25 °C for 48 h. The swelling ratio, SR, of scaffold was calculated according to the equation 1 below,

$$SR = \frac{W_h - W_d}{W_d} \qquad (1)$$

35 where W_h is the weight of the scaffold in the swollen equilibrium and W_d is the weight of the dried scaffold. Each sample was measured three times from the four replicate specimens and the average value of the measurement was taken.

Compression test was carried out to determine the mechanical
40 properties of hydrated scaffolds with different polymer concentrations using a dynamic mechanical analyzer (TA Instruments, Q800) at a frequency of 1 Hz and a preload of 0.01 N. The testing was performed under atmospheric condition and 298 K. The compression testing was performed in quadruplicate.

45

Interior morphology, porosity and mercury intrusion porosimetry

The lyophilised sample of different polymer concentrations were fractured carefully and their interior morphology was studied by
50 using a scanning electron microscope (SEM) (FEI Quanta 200 ESEM with EDAX Si(Li) X-ray detector and Gatan Alto Cyro stage) after the sample have been coated with gold and palladium for 30 s.

The interconnecting pores in the HPC-MA scaffold were
55 assessed by performing Focused Ion Beam (FIB) milling to probe the scaffold interiors, similar to the approach detailed in Al-Abboodi et al[29]. All FIB/SEM experiments were based on Helios Nanolab 600 (FEI company), and a highly focused ion beam (30 kV, Ga+) of large current (21 nA) was used to ablate an area of
60 approximately 500 × 500 μm on the scaffolds. The ablation process was continuously monitored by SEM, until an ablation depth close to 50 μm has been achieved.

The porosities of the scaffolds were determined using the solvent replacement method. In brief, lyophilised samples were
65 first submerged in absolute ethanol for 24 h, and weighted after excess ethanol on the surface was blotted. Each sample was measured three times from the four replicate specimens and the average value of the measurement was taken. The porosity of the scaffold was calculated according to the equation 2 below,

70

$$Porosity = \frac{M_h - M_d}{\rho V_t} \times 100\% \qquad (2)$$

where M_d and M_h are the weight of scaffold before and after the immersion in absolute ethanol respectively. ρ is the density of absolute ethanol and V_t is the total volume of the scaffold.
75 The pore size distribution was determined using a mercury intrusion porosimetry (MIP) method. The interconnected pore size distribution of the lyophilised scaffold was measured out by carefully fractured into the desired size and weight before testing using a mercury porosimeter (Autopore III, Micromeritics Co.).

80

Degradation study

Degradation study was carried out using the HPC-MA hydrogel disks at different concentrations with dimensions of 1 cm diameter and 1 mm thickness. It is known that polymer
85 containing ester linkage undergoes hydrolysis in the present of phosphate buffered saline solution (PBS)[30, 31], therefore, the degradation study of HPC-MA hydrogel contains hydrolytically degradable methacrylate pendant group (ester linkage) was carried out in PBS solution. The hydrogel disks were incubated in
90 5 mL of PBS (pH 7.4) at 37 °C and shaken at 150 rpm for 40 days in a shaking incubator. The PBS solution was replaced every 5 days throughout the study. At pre-determined time points (5 days), the samples were rinsed with deionised water, dried in a vacuum oven for 48 h at 40 °C. Their weight loss was then
95 recorded. These experiments were performed with four replicates.

Surface functionalization of scaffold and cell culture of adipose-derived stem cells (ASCs)

Lyophilised HPC-MA-10 wt% scaffolds were decontaminated by
100 soaking in 70% ethanol overnight followed by washing with sterile phosphate buffered saline (PBS) before surface functionalisation. Sterilized scaffolds were activated in 40 nM 1,1'-carbonyldiimidazole (CDI) in acetone at room temperature for 3 h. The activated scaffolds were then washed in acetone for 3
105 to 4 times to remove any unreacted traces of CDI. After washing, the activated scaffolds were treated with gelatin (1.16 mg mL⁻¹) in a sodium bicarbonate (NaHCO₃) buffer (50 mM, pH 9) at room temperature for 24 h. The conjugated scaffolds were washed

twice with sterile PBS before lyophilisation.

StemPro® human derived stem cells (P3) were cultured in a complete media comprising of Dulbecco's Modified Eagle Medium Nutrient Mixture F-12 (DMEM-F12), supplemented with 10 % Fetal Bovine Serum, 1 % non Essential Amino Acid, 1 % L-glutamine and 1 % P/S solution at 37 °C in a humidified atmosphere of 5 % CO_2 (all chemicals and cells were obtained from Life Technologies). The media was changed every 48 h.

ASCs were trypsinised using 0.25% trypsin upon confluence and seeded onto the sterilized scaffolds. The scaffolds were decontaminated by immersion in ethanol for 24 h with subsequent change of ethanol every 4 h, followed by rinsing in phosphate buffered saline (Life Technologies) and final immersion in DMEM-F12 solution. The scaffolds were subsequently dried and 30 µl of cell suspension was added dropwise at a density of 34,000 cells/cm^3 to the scaffold. After 4 hours, complete media was added for subsequent culture. Adipogenesis of ASCs in the scaffolds was also carried out by supplementing the cells with adipogenic media. The media was changed every 3 days.

Morphology and proliferation of ASCs in scaffolds

The surface and cross-sectional morphologies of the scaffolds as well as ASCs morphology after 14 days of *in vitro* culture were analysed using the scanning electron microscopy (SEM) (JEOL JSM-5410, Japan). The cell-scaffolds were first fixed in 2.5% gluteraldehyde for 2 h, followed by a series of dehydration in graded ethanol (50%, 70%, 80%, 90%) with 15 min incubation at each interval, and final immersion in 100% ethanol for 30 min. Hexamethyldisilazane was subsequently added to the scaffolds and left to incubate for 1 h before removal and left for overnight drying at room temperature. The scaffolds were subsequently frozen in liquid nitrogen before being freeze-fractured into several sections and coated with gold prior to imaging. An acceleration voltage of 5 kV was used and images were obtained at different magnifications.

The capability of ASCs to proliferate in the scaffolds was analyzed using the alamarBlue® assay on days 2, 4 and 7. At each time point, 200 µl of 10% alamarBlue® dye (diluted with complete medium) was added to each scaffold and incubated for 4 h at 37°C in a humidified atmosphere of 5 % CO_2. Fluorescence analysis using an excitation wavelength of 570 nm and emission wavelength of 585 nm was carried out with Thermoscientific Varioskan Flash Multimode Reader. The number of cells corresponding to the particular relative fluorescence unit (RFU) was subsequently obtained from the standard curve (plot of RFU vs. known cell numbers).

Adipogenic characterization of ASCs and gene expression (RT-PCR)

Day 2, 4, 7 and 14 cell cultured scaffolds were fixed in 4% paraformaldehyde (Sigma-Aldrich) for 30 min and cryosectioned into thin sections of 30 µm each. 200 µl of 60% Oil Red O stain (Sigma-Aldrich) was added onto the sections and left to incubate for 5 min before imaging under the light microscope (Carl Zeiss Primo Vert).

Adipogenesis of ASCs in the scaffolds was also determined by quantifying the amount of adiponectin and leptin released over a period of 14 days using Human Adiponectin and Leptin ELISA assay kits (Raybiotech). All media was collected at each media change and frozen at -80 °C before testing. The assays were performed according to manufacturer's instructions. Fluorescence analysis was carried out at 450 nm using the Gemini EM Microplate Reader.

Adipogenic differentiation of ASCs after 14 days of culture in the adipogenic medium was also confirmed by RT-PCR analysis. Undifferentiated ASCs cultured in complete DMEM-F12 media was also used as a control. Scaffolds were homogenized in trizol reagent and the RNA was extracted using the Total RNA kit I (Omega Bio-Tek). The cDNA was synthesized from the total RNA using iScript™ cDNA Synthesis Kit (Biorad). The cDNA was used as the template in a 20 µl reaction mixture containing specific primer pair of each cDNA according to the sequences with SYBR® Green Supermix (Biorad) (Table 1) for PCR analysis. The mRNA levels were normalized to those of GAPDH, and changes in gene expression were calculated as fold changes (the $\Delta\Delta Ct$ method).

Table 1 PCR primers

Gene	5' to 3' Sequence (sense)	5' to 3' Sequence (antisense)
GAPDH	CCCCTTCATTGACCTCAACTACA	TTGCTGATGATCTTGAGGCTGT
PPARG	CTCCTATTGACCCAGAAAGC	GTAGAGCTGAGTCTTCTCAG
LPL	ATGGAGAGCAAAGCCCTGCTC	GTTAGGTCCAGCTGGATCGAG
Leptin	GTGCC-TATCCAGAAAGTCCAG	TCAGCATTCAGGGCTAACA TC
Adiponectin	CATGACCAGGAAACCACGACT	TGAATGCTGAGCGGTAT

Statistical Analysis

All experiments were performed in at least three replicates. Results were reported as average value ± standard deviation. One-way analysis of variance (ANOVA) was used to compare multiple groups of data statically; p values lower than 0.05 were considered statistically significant.

Results and discussion

HPC-MA characterization and hydrogel preparation

HPC-MA conjugate was synthesized by modifying HPC by MA as depicted in Fig. 1a. The degree of substitution (DS) was ~ 0.35 as calculated by ^1H NMR in $CDCl_3$. ^1H NMR ($CDCl_3$, δppm): 0.5-1.5 ($-CH_3-CH-$), 1.8-2.0 ($CH_3-C=CH_2$), 5.5-6.2 ($-C=CH_2$), 2.5-5.3 (other protons) (Fig. 1b). The degree of modification is defined as the substitution degree of available -OH groups on the HPC chain. Fig. 1c demonstrated that the HPC-MA retains the phase behaviour characteristic of HPC. The LCST of HPC-MA was determined to be approximately 40 to 41 °C, after which the transmittance decreases drastically with increasing temperature until reaching a plateau at ~45°C. HPC-MA with 0.35 DS was selected as an example for scaffold preparation. Porous HPC-MA hydrogel was produced using simple procedures without the use of porogens as illustrated in Fig. 1d. HPC-MA conjugates with

0.35 DS are water-soluble and formed single-phase solution when dissolved in aqueous solution (Fig. 1d Step 1). HPC-MA exhibited low critical solution temperature (LCST) transition at around 40°C. Upon heating the solution above its LCST, HPA-
5 MA solution underwent phase transition from isotropic solution to colloidal solution (Fig. 1d Step 2). Fixation of the colloidal structure of HPC-MA was achieved by polymerizing the HPC-MA conjugate and produced an opaque hydrogel (Fig. 1d Step 3). UV-irradiation was selected to induce photopolymerisation due to
10 its many advantages including fast polymerization rate at low temperature, and ease of hydrogel shaping[32], Irgacure 2959 has been demonstrated to cause minimal toxicity to a wide range of mammalian cells[33], and was employed as a photoinitiator in this study. Further lyophilisation of the hydrogel produced highly
15 porous structures (Fig. 1d Step 4). HPC-MA-10 %, HPC-MA-15 % and HPC-MA-20 % hydrogel samples were prepared and subjected to characterization, and will be described in later sections.
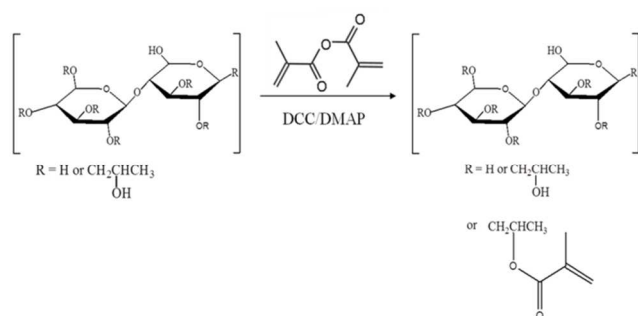
20   **Fig. 1a** Synthesis scheme of HPC-MA
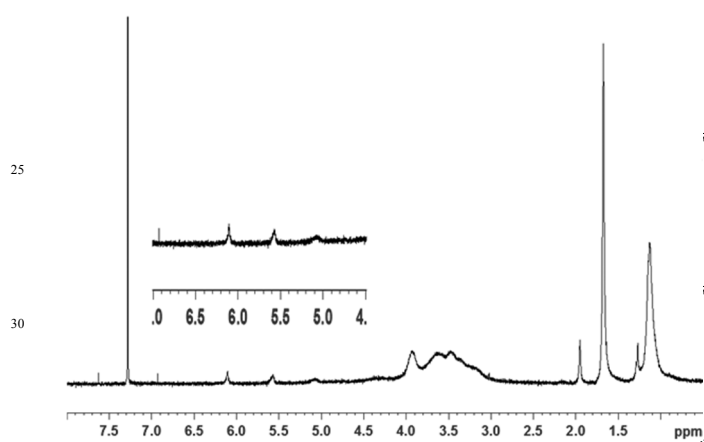
Fig. 1b NMR of HPC-MA in CDCl$_3$
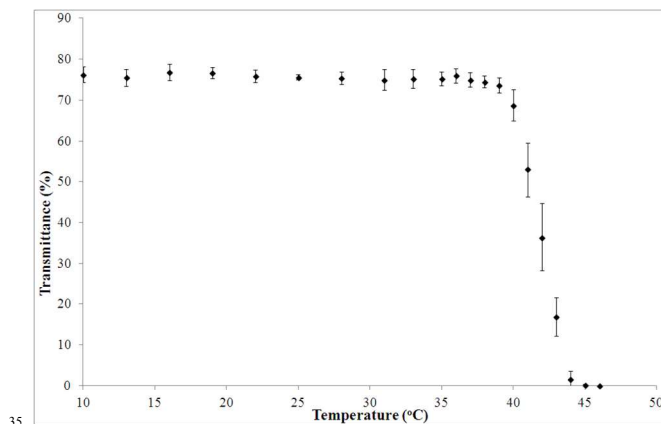
35 **Fig. 1c** Turbidimetry measurement for HPC-MA-10 wt%. The data are shown as mean values with standard deviation as error bars in the form of mean value ± standard deviation.
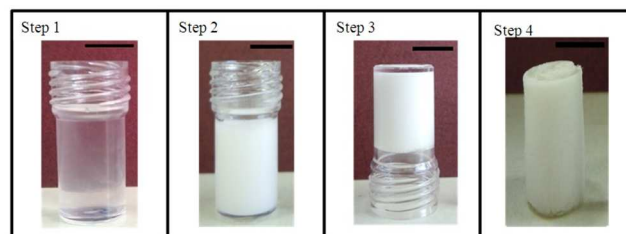
40 **Fig. 1d** Preparation of HPC-MA scaffold (scale bar 1.0 cm) from (Step 1) homogenous solution of HPC-MA-10 wt% at room temperature, to (Step 2) phase separated colloidal fluid at ~ 45 ºC, (Step 3) crosslinked heterogeneous gel at room temperature and (Step 4) freeze-dried scaffold.

Swelling ratio and mechanical properties

45 Fig. 2 summarizes the swelling ratios (SR) of the lyophilised HPC scaffolds in water and the storage modulus of hydrated HPC-MA at room temperature. Swelling ratio is a measure of wettability of a material. Hydrogels with high swelling ratio are highly permeable, which facilitates oxygen, nutrient and
50 metabolites exchange, and are considered as promising material for tissue scaffolding[34]. It was seen that the three different HPC-MA concentration exhibits high SR attributed to the presence of hydroxyl groups on the HPC chain that attract water molecules from the surrounding environment. The SR was found to be
55 decreasing with increasing HPC-MA concentration (p < 0.05, n = 4), whereas HPC-MA-10% had the highest SR of 35.83 while the SR of HPC-MA-15% and HPC-MA-20% were found to be 19.16 and 12.94, respectively. It is well known that crosslinking density has a strong influence on the swelling ratio of hydrogel[35-39]. The
60 number of crosslinking bonds per volume, known as crosslinking density, increases with increasing polymer concentration. As the crosslinking density increases, the water molecules and water-soluble substances will find it hard to infiltrate into a densely crosslinked network, thus, resulting in lower swelling ratio.

65   Biological tissues and organs are soft viscoelastic materials, which display a wide range of mechanical properties tailored for their specific physiological function. Change in tissue stiffness is generally associated with pathological disease or tissue dysfunction[10, 40]. Accumulative evidences suggest that substrate
70 mechanics and the topography of extracellular microenvironment can regulate cell phenotype similar to the influence of biochemical signals[41, 42]. Mechanical strength is therefore an

important property of hydrogel scaffold. For tissue regeneration to be successful, it is believed that the mechanical properties of scaffold should match roughly the mechanical properties of tissue growth in order to provide cells with instructive microenvironment. The storage modulus of HPC-MA-10%, 15% and 20% were found to be 0.75, 1.87 and 4.28 KPa, respectively. As expected, the storage modulus increased with increasing HPC-MA concentration ($p < 0.05$, n = 4). It is well known that hydrogel with higher precursor mass exhibit stronger mechanical properties, as the crosslinking degree increases due to formation of longer attached chain[36, 43]. The storage modulus of the HPC-MA hydrogels are comparable to that of soft tissues and organs such as brain, lymph node, mammary gland, liver, breast tumor and kidney[10], and suggesting that the HPC-MA hydrogels can be used as tissues scaffolds to mimic these soft tissues. These results prove that the swelling ratio and mechanical properties of the hydrogel can be tuned by altering the crosslinking density[36].
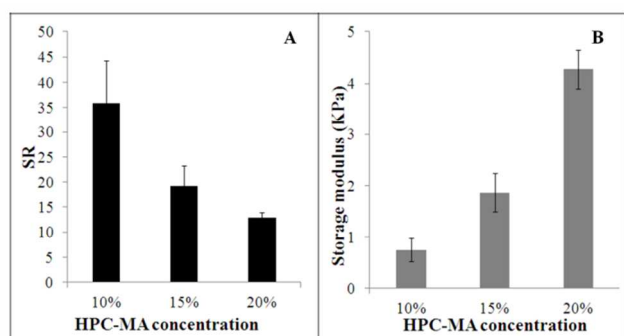
Fig. 2 Swelling ratio (A) and storage modulus (KPa) (B) of HPC-MA-10 wt%, 15 wt% and 20 wt% hydrogels at room temperature respectively. The data are shown as mean values with standard deviation as error bars in the form of mean value ± standard deviation.

Physiochemical properties of hydrogels

HPC-MA scaffold with interconnected porous structure was fabricated by polymerizing colloidal HPC-MA solution followed by lyophilisation. It is well known that polymerization in colloidal solution generates open-cell structure i.e. interconnected porous structure with water channels throughout the network[43, 44]. Fig. 3A-F shows the cross sections of the three different concentrations of lyophilised HPC-MA scaffolds visualized and characterized using SEM at low and high magnification. As expected, the SEM images revealed that all the HPC-MA scaffolds were highly porous with interconnected pores. The degree of interconnection was assessed by mercury porosimetry and Focused ion bean milling - scanning electron microscopy (FIB-SEM). The mercury porosimeter method is a common technique used by many groups to quantify interconnected porosity, as mercury porosimetry only measures the interconnected channels in a microstructure, the result has therefore been used to verify the interconnectivity of a microstructure[45-49]. FIB milling has been used as a new technique to assess the 3D porosity of hydrogel[29], the FIB/SEM also allows a precise visualization of the interconnectivity of scaffold. Representative images in Fig. 4a (A) and (B) showed the cross-section of HPC-MA-10% before FIB milling and after a 50μm

layer has been removed, respectively. Interconnections between different pores in these two layers were observed, which further verified the interconnectivity of the scaffolds. Such interconnected pores are needed for cell infiltration, unrestricted cell-cell signalling, and nutrient transport to take place. Mercury porosimeter measurements further confirmed the presence of highly interconnected macroporous structure in HPC-MA-10%, 15 wt% and 20 wt%. Representative pore size distribution graphs are shown in Fig. 4b. All scaffolds had pore size ranging from 30 to 330 μm. HPC-MA-10%, HPC-MA-15% HPC-MA-20% exhibited median mean pore diameter of 69.4, 45.1, and 42.4 μm, respectively. The pore size of HPC-MA scaffold depends on the polymer concentration as expected. It was found that a decrease in the average value of median pore size ($p < 0.05$, n = 4) was associated with increase in polymer concentration as expected. It is well known that high crosslinking density will result in smaller pore size due to the highly intramolecularly crosslinked copolymers[50]. Nonetheless, all three scaffolds were highly porous. The interconnected porosities determined by mercury intrusion porosimetry for HPC-MA-10%, HPC-MA-15%, and HPC-MA-20% were found to be 93±0.8 %, 94±0.7, and 96±0.9 %, respectively. There is no significant difference between the porosity measurements obtained using solvent replacement method and the porosity measurements obtained using mercury intrusion porosimetry ($p > 0.05$, n = 4). These results suggest that induced phase separation technique is able to create highly interconnected macroporous and high porosity 3D structure.
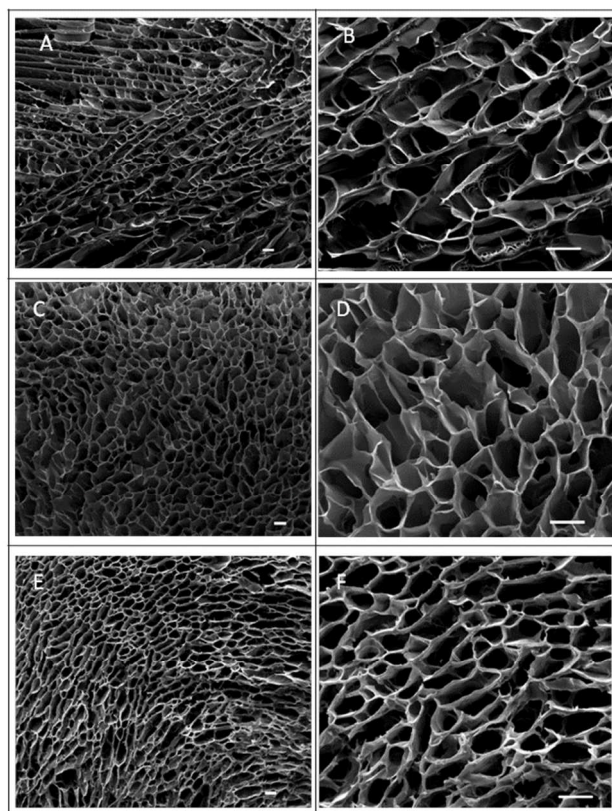

Fig. 3 Pore size and morphology of HPC-MA scaffolds. (A) and (B), (C) and (D), (E) and (F) are representative cross-sectional SEM micrographs of lyophilised HPC-MA-10 wt%, 15 wt% and 20 wt% , at low and high magnification (scale bar 100 μm), respectively.
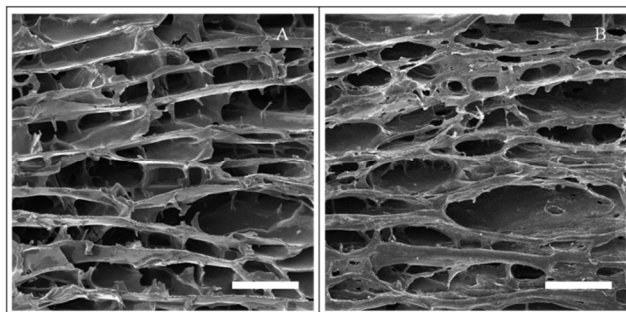
Fig. 4a FIB/SEM of HPC-MA-10 wt% (scale bar 100 μm), top view SEM image of the scaffold before milling (A), after a layer of approximately 50 μm in thickness milled off by FIB (B).
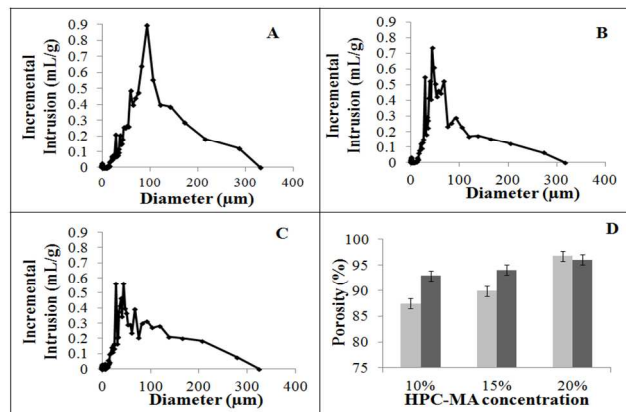

5

Fig. 4b Pore size distribution of HPC-MA-10 wt% (A), 15 wt% (B) and 20 wt% (C); Porosity (▢) and interconnected porosity (▪) of HPC-MA scaffold (D). The data are shown as mean values with standard deviation as error bars in the form of mean value ± standard deviation.

10

Degradation profile

For successful tissue regeneration, a tissue scaffold should provide sufficient mechanical support for cell proliferation before new tissue growth, but it should degrade and resorb at a rate that
15 matches the new tissues growth rate[51]. Cellulose possesses many favourable properties that make it attractive as a tissue scaffold materials[26]. However, cellulose is generally regarded to have limited in vivo degradability due to the absence of appropriate hydrolases. The subcutaneous implantation of cellulose sponge
20 was studied[52] and a decrease in implant size was observed after 16 weeks, however it is suggested that the complete disappearance of cellulose sponge will take longer than 60 week. The degradation of an allyl isocynate modified HPC hydrogel was studied[26] over a period of 12 weeks and observed no
25 significant degradation. To improve the degradability of HPC hydrogel, a bifunctional linker MA was incorporated into HPC as pendant group. It is well known that MA can be radically polymerized to form polyester network and the resulting ester linkages are hydrolytically degradable[53, 54]. The hydrolytic
30 degradation of HPC-MA hydrogels was monitored by measuring the weight loss of samples over time, and the results were presented in terms of weight percentage remaining against time. Fig. 5 shows the degradation profile of HPC-MA hydrogels with different polymer concentration over a period of 40 days in PBS.
35 All HPC-MA hydrogels underwent degradation after 5 days of

incubation in PBS, indicating that the use of degradable crosslinker methacrylate anhydride has greatly improved the degradability of cellulose hydrogel. The degradation of HPC-MA-10% was the fastest with a remaining weight of
40 approximately 10% after 40 days. The percentage of remaining weight of HPC-MA-15% was approximately 30% after 40 days, whereas the percentage of remaining weight of HPC-MA-20% was approximately 50% after 40 days. As expected, the hydrogels prepared from higher HPC-MA concentration showed slower
45 degradation ($p < 0.05$, n = 5). It is known that polyesters degrades by hydrolytic cleavage of the ester linkage, the degradation rate is highly dependent on the crosslinking density[55, 56]. The degradation is slower in tightly crosslinked network due to the lower water accessibility, hence slower hydrolysis rate. The data
50 obtained in this work illustrates that varying the polymer concentration can alter the degradation rate of HPC-MA hydrogel.
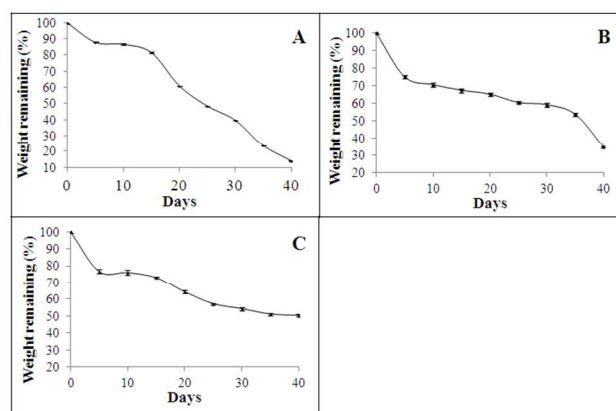

Fig. 5 Degradation profile of HPC-MA-10 wt% (A), 15 wt% (B) and 20
55 wt% (C). The data are shown as mean values with standard deviation as error bars in the form of mean value ± standard deviation, and the standard deviations appear to be small.

Surface functionalization of scaffold and cell proliferation in
60 hydrogel scaffold

Most mammalian cells are anchorage dependent, therefore, cell adhesion to the extracellular matrix (ECM) plays important role in regulating cell survival, cell cycle progression, tissue-specific phenotype expression, organogenesis, wound healing, tissue
65 homeostasis and remodelling[57]. An ideal tissue scaffold should provide cell adhesion sites. HPC as a commercial derivate of cellulose has many favourable properties as biomaterials[23, 58], but it does not contain any cell-recognizable signal molecules that can mediate mammalian cell adhesion. To achieve cell-substrate
70 interaction, the scaffold surface can be functionalized with biochemical cues after scaffold fabrication[59]. To demonstrate the feasibility to introduce biochemical cues to the HPC-MA hydrogel to enable cell adhesion, the surface of HPC-MA-10% was activated by CDI followed by conjugation with gelatin.
75 Gelatin contains arginine-glycine-aspartate (RGD) peptide sequence that can mediate cell-substrate interaction[34, 60]. To evaluate the feasibility of using HPC-MA hydrogels as 3D scaffold for adipose tissue engineering, ASCs were cultured for 21 days in the scaffold with adipogenic medium and analyzed

using SEM. Fig. 6A and 6B show the presence of ASCs on the surface and cross section of scaffolds, respectively.. These results indicated that the HPC-MA scaffold supported the growth of ASCs, as well as infiltration into the scaffold (Fig. 6B),
5 demonstrating its high-interconnected porosity. In addition, using alamarBlue® as an indirect indicator of cell proliferation, the number of ASCs was observed to increase gradually over a period of 7 days from the cell proliferation data, which indicated that the material properties of the scaffold supported the growth
10 of ASCs (Fig. 7). It is noted that cells are seeded onto HPC-MA scaffolds using a typical static seeding method which may not result in optimal seeding efficiency or optimal cell distribution. In subsequent study, alternative cell seeding method such as surface acoustic wave driven seeding method[61] can be employed to
15 improve the seeding efficiency.
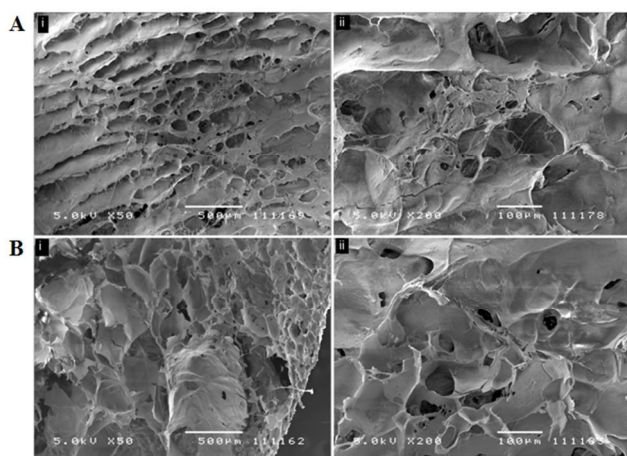
Fig. 6 SEM micrographs illustrating the presence of ASCs on the (A)
20 surface and (B) cross-section of Day 14 cell cultured HPC-MA-10 wt% scaffolds at (i) 50X and (ii) 200X magnifications.
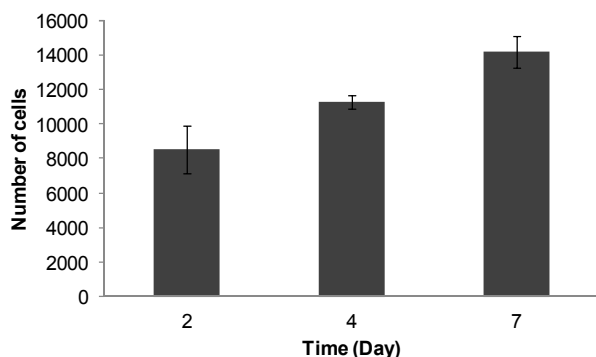
Fig. 7 Number of ASCs in the HPC-MA-10 wt% scaffolds over a period of one week.

25 **Adipogenic characterization**

The differentiation capability of ASCs that were cultured in the scaffolds with adipogenic supplements was also studied. It is very well known that adipogenesis is enhanced on scaffolds with stiffness similar to that of in vivo adipose tissue[62, 63]. After
30 studying the mechanical characterization results above, HPC-MA-10% was selected for this study since it exhibits a storage

modulus closest to that of adipose tissue[64] in comparison to the other two scaffold formulations. Adipogenic differentiation of ASCs into adipocytes inside the scaffolds was evaluated by Oil
35 Red O (ORO) staining[65]. Fig. 8A illustrates the typical ORO staining image of a fat tissue, while Fig. 8B-C show the oil content of Day 14 ASCs grown on a two-dimensional (2D) tissue culture plate (TCP) without and with adipogenic medium, respectively. It was observed that ASCs did not differentiate into
40 adipocytes in the absence of adipogenic medium. From Fig. 8c, an increase in the oil content in the ASCs grown in the scaffolds could be observed over a period of 14 days. From the results, an absence of stained lipid content was observed on Day 2, thereby showing the absence of adipogenesis at this initial stage. From
45 Day 4 onwards, lipid droplets that were stained red were observed and the amount of lipid content increases with longer period of culture. A large amount of oil content was observed on Day 14. Adipogenic differentiation of ASCs into adipocytes in the scaffolds was further confirmed by the release of adiponectin
50 and leptin into the medium. Similar to ORO staining, both adiponectin (Fig. 9A) and leptin (Fig. 9B) release began on Day 4, and the amount of adiponectin and leptin released increased significantly after 14 days of culture ($p<0.05$, n=3). In addition, the amount of adiponectin released was much higher than leptin
55 over the same period of time. Hence, ASCs were also capable of differentiating into adipocytes in the scaffolds. Evidence is emerging that physical culture conditions play a major role in determining stem cell fate to an extent that surpasses the influence of growth and differentiation factors[66-68]. Of particular
60 relevance to this work is the discovery that geometric factors play important role in regulating the commitment of stem cell fate. For instant, well-spread mesenchymal stem cells (MSCs) underwent osteogenesis, while un-spread cells underwent adipogenesis[69, 70]. Ruiz & Chen demonstrated that MSCs underwent osteogenesis at
65 convex edges and adipogenesis at concave edges[71]. It was observed that the HPC-MA scaffolds contain large number of concave pores as compared to convex edges, the provision of large number of concave pores in HPC-MA scaffolds may also promote adipogenesis of ASCs.
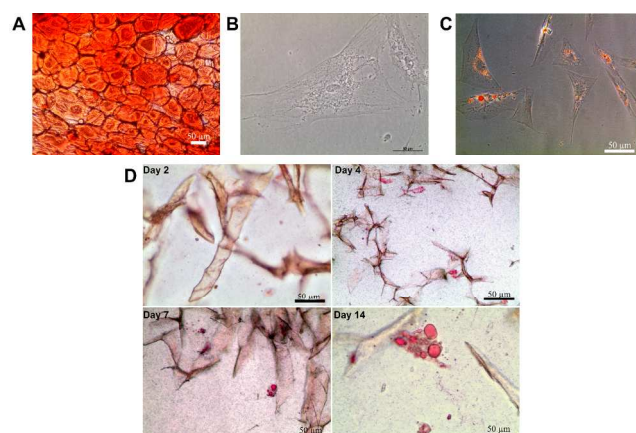

70

Fig. 8 Oil Red O staining of the lipid droplets of (A) fat tissue, (B) ASCs grown on 2D TCP without adipogenic supplement, (C) ASCs grown on 2D TCP with adipogenic supplment (Day 14), and (D) ASCs grown in the 3D HPC-MA-10 wt% scaffold over a period of 14 days and lipid droplets
75 were observed to be present from Day 4 onwards. Scale bar 50μm.
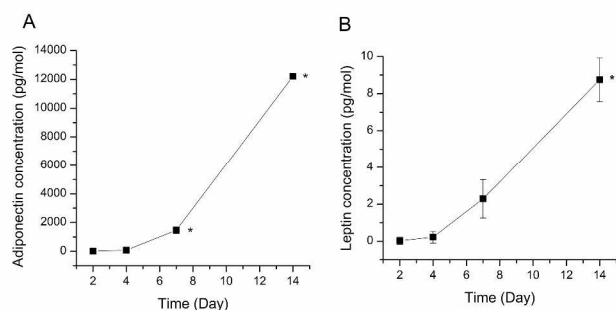
Fig. 9 Amount of (A) adiponectin and (B) leptin released into the medium over a period of 14 days. Both adiponectin and leptin were released from Day 4 onwards, and the amount released increased significantly after 14
5 days of culture (*$p<0.05$, n=3). The data are shown as mean values with standard deviation as error bars in the form of mean value ± standard deviation, and the standard deviations appear to be small.

Gene expression (RT-PCR)

10 Adipogenic differentiation of ASCs in the scaffolds was further confirmed by evaluating the gene expression levels of adipogenic markers. The fold change values for ASCs cultured with adipogenic supplements in the scaffold was compared to the undifferentiated ASCs cultured on TCP (control) for the
15 adipogenic genes (PPARG, LPL, leptin and adiponectin). ASCs subjected to differentiation in the scaffold displayed fold change values that were much higher than the control for early adipogenic markers (PPARG and LPL) ($p<0.05$, n=3) (Fig. 10A) and late adipogenic markers (adiponectin and leptin) ($p<0.05$,
20 n=3) (Fig. 10B). The upregulation of adipogenic stem cell markers suggests that the 3D scaffold together with the adipogenic supplements led to the differentiation of ASCs into adipocytes. The successful adipogenesis could also be attributed to the use of a 3D matrix with mechanical stiffness matching that
25 of native adipose tissue. It is worthwhile to mention that scaffold mechanical properties
play an important role in directing stem cell niche and ASCs
are capable of differentiating into a variety of cell types not limiting to adipocyote[9, 13, 14]. In subsequent study, HPC-MA
30 scaffolds with higher storage modulus can be employed as 3D adipose stem cells culture system. The effect of increasing storage modulus of scaffold on adipose stem cell fate is currently under investigation.
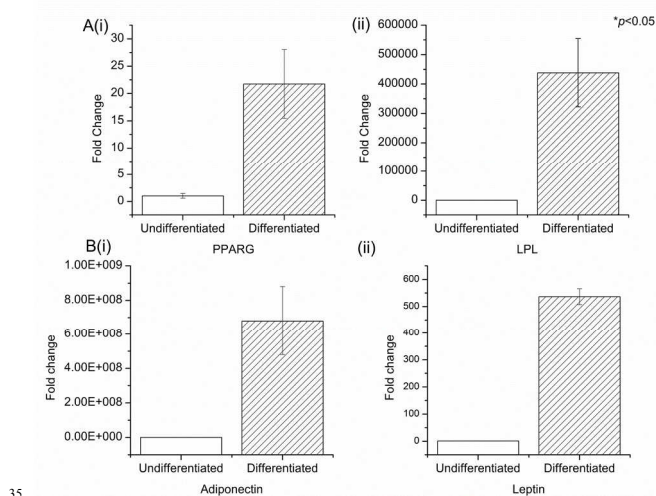

Fig. 10 PCR results for ASCs cultured in the scaffolds with adipogenic supplements compared to undifferentiated ASCs cultured on TCP (control). Fold change values of the samples were shown for (A) early
40 adipogenic markers (i) PPARG and (ii) LPL, and (B) late adipogenic markers (i) adiponectin and (ii) leptin. The upregulation of adipogenic markers suggests that the 3D microenvironment together with the adipogenic supplements led to the differentiation of ASCs into adipocytes (*$p<0.05$, n=3).

45 ## Conclusions

In this study, a novel class of 3D macroporous hydroxypropyl cellulosic scaffolds were developed by UV polymerizing MA conjugated HPC at its biphasic phase. The scaffolds exhibited high swelling ratio, biodegradability, cytocompatibility, and
50 mechanical integrity similar to that of soft tissue in particularly adipose tissue. The pore structure of HPC-MA scaffolds was highly interconnected as a result of the use of phase separation technique followed by lyophilisation. By applying the same principle, macroporous scaffolds can be prepared using other
55 responsive polymers that can form colloidal system induced by environmental stimuli such as temperature and pH change. The HPC-MA scaffolds promoted ASC infiltration, proliferation and adipogenesis. Hence, these interconnected macroporous hydrogels are promising 3D in vitro adipocyte culture systems
60 that can be used for studying tissue-inherent interactions such as 3D cell-matrix interactions.

Acknowledgements

Notes and references

a Department of Chemical Engineering, Monash University, Australia. Email: siew.hoo@monash.edu.
b MicroNanophysics Research Laboratory, School of Applied Science, RMIT University, Australia. Tel: +613 9925 2660. Email:
5 *peggy.chan@rmit.edu.au*
c Melbourne Centre for Nanofabrication, Clayton, Australia
d School of Materials Science and Engineering, Nanyang Technological University, Singapore.Fax: +65 6790 908. Tel: +65 6513 8166. Email: cleochoong@ntu.edu.sg
10 *e ARC Centre of Excellence for Electromaterials Science, Intelligent Polymer Research Institute, AIIM facility University of Wollongong, Australia. Email: zyue@uow.edu.au*
f Department of Mechanical and Aerospace Engineering, Monash University, Australia. Email: jing.fu@monash.edu
15 *g School of Chemical & Biomedical Engineering, Nanyang Technological University, Singapore. Email: TYTan@ntu.edu.sg*
† Electronic Supplementary Information (ESI) available: [details of any supplementary information available should be included here]. See DOI: 10.1039/b000000x/

20

1. P. Bauer-Kreisel, A. Goepferich and T. Blunk, *Advanced drug delivery reviews*, 2010, **62**, 798-813.
2. M. L. Moya, M. H. Cheng, J. J. Huang, M. E. Francis-Sedlak, S. W. Kao, E. C. Opara and E. M. Brey, *Biomaterials*, 2010, **31**, 2816-
25   2826.
3. E. Thian, J. Huang, M. Vickers, S. Best, Z. Barber and W. Bonfield, *Journal of Materials Science*, 2006, **41**, 709-717.
4. S. Q. Liu, R. Tay, M. Khan, P. L. Rachel Ee, J. L. Hedrick and Y. Y. Yang, *Soft Matter*, 2010, **6**, 67-81.
30 5. C. T. Gomillion and K. J. L. Burg, in *Comprehensive Biomaterials*, ed. D. Editor-in-Chief: Paul, Elsevier, Oxford, 2011, pp. 529-539.
6. E. Sachlos and J. T. Czernuszka, *European cells & materials*, 2003, **5**, 29-39; discussion 39-40.
7. T. B. Woodfield, J. Malda, J. de Wijn, F. Peters, J. Riesle and C. A.
35   van Blitterswijk, *Biomaterials*, 2004, **25**, 4149-4161.
8. R. A. Marklein and J. A. Burdick, *Adv Mater*, 2010, **22**, 175-189.
9. L. E. Flynn, *Biomaterials*, 2010, **31**, 4715-4724.
10. I. Levental, P. C. Georges and P. A. Janmey, *Soft Matter*, 2007, **3**, 299-306.
40 11. J. M. Gimble, A. J. Katz and B. A. Bunnell, *Circulation research*, 2007, **100**, 1249-1260.
12. B. Lindroos, R. Suuronen and S. Miettinen, *Stem cell reviews*, 2011, **7**, 269-291.
13. H. Mizuno, *Journal of Nihon Medical School = Nihon Ika Daigaku*
45   *zasshi*, 2009, **76**, 56-66.
14. P. A. Zuk, M. Zhu, P. Ashjian, D. A. De Ugarte, J. I. Huang, H. Mizuno, Z. C. Alfonso, J. K. Fraser, P. Benhaim and M. H. Hedrick, *Molecular biology of the cell*, 2002, **13**, 4279-4295.
15. B. Galateanu, S. Dinescu, A. Cimpean, A. Dinischiotu and M.
50   Costache, *International Journal of Molecular Sciences*, 2012, **13**, 15881-15900.
16. G. L, K.-V. N, B. K and B. A, *Folia Biologica* 2011, **57**, 47-56.
17. L. Flynn and K. A. Woodhouse, *Organogenesis*, 2008, **4**, 228-235.
18. F. J. O'Brien, B. A. Harley, I. V. Yannas and L. J. Gibson,
55   *Biomaterials*, 2005, **26**, 433-441.
19. S. H. Oh, I. K. Park, J. M. Kim and J. H. Lee, *Biomaterials*, 2007, **28**, 1664-1671.
20. M. Sabir, X. Xu and L. Li, *Journal of Materials Science*, 2009, **44**, 5713-5724.
60 21. B. Subia, J. Kundu and S. C. Kundu, *Tissue Engineering*, 2010, 524.

22. Y. Ikada, *Tissue Engineering: Fundamentals and Applications*, Interface Science and Technology, Elsevier, 2006.
23. J. L. Drury and D. J. Mooney, *Biomaterials*, 2003, **24**, 4337-4351.
24. Q. Cai, J. Yang, J. Bei and S. Wang, *Biomaterials*, 2002, **23**, 4483-
65   4492.
25. N. Soykeabkaew, C. Sian, S. Gea, T. Nishino and T. Peijs, *Cellulose*, 2009, **16**, 435-444.
26. Z. Yue, F. Wen, S. Gao, M. Y. Ang, P. K. Pallathadka, L. Liu and H. Yu, *Biomaterials*, 2010, **31**, 8141-8152.
70 27. M. A. Hussain, *Journal of Polymer Science Part A: Polymer Chemistry*, 2008, **46**, 747-752.
28. J. M. Pachence, M. P. Bohrer and J. Kohn, in *Principles of Tissue Engineering (Third Edition)*, eds. L. Robert, L. Robert, R. L. Joseph VacantiA2 - Robert Lanza and V. Joseph, Academic Press,
75   Burlington, 2007, pp. 323-339.
29. A. Al-Abboodi, J. Fu, P. M. Doran and P. P. Y. Chan, *Biotechnology and Bioengineering*, 2013, **110**, 318-326.
30. W. Dong, H. Li, M. Chen, Z. Ni, J. Zhao, H. Yang and P. Gijsman, *J Polym Res*, 2011, **18**, 1239-1247.
80 31. G. D. Nicodemus and S. J. Bryant, *Tissue engineering. Part B, Reviews*, 2008, **14**, 149-165.
32. R. S. Benson, *Nuclear Instruments and Methods in Physics Research Section B: Beam Interactions with Materials and Atoms*, 2002, **191**, 752-757.
85 33. C. G. Williams, A. N. Malik, T. K. Kim, P. N. Manson and J. H. Elisseeff, *Biomaterials*, 2005, **26**, 1211-1218.
34. L.-S. Wang, J. E. Chung, P. Pui-Yik Chan and M. Kurisawa, *Biomaterials*, 2010, **31**, 1148-1157.
35. M. Davidovich-Pinhas and H. Bianco-Peled, *Carbohydrate*
90   *Polymers*, 2010, **79**, 1020-1027.
36. F. Lee, J. E. Chung and M. Kurisawa, *Journal of Controlled Release*, 2009, **134**, 186-193.
37. W.-F. Lee and W.-H. Chiang, *Journal of Applied Polymer Science*, 2004, **91**, 2135-2142.
95 38. D. Singh, D. Kuckling, V. Koul, V. Choudhary, H.-J. Adler and A. K. Dinda, *European Polymer Journal*, 2008, **44**, 2962-2970.
39. D. Wang, D. J. T. Hill, F. Rasoul and A. K. Whittaker, *Radiation Physics and Chemistry*, 2011, **80**, 207-212.
40. W. L. K. Chen and C. A. Simmons, *Advanced drug delivery reviews*,
100   2011, **63**, 269-276.
41. G. C. Reilly and A. J. Engler, *Journal of biomechanics*, 2010, **43**, 55-62.
42. L.-S. Wang, J. Boulaire, P. P. Y. Chan, J. E. Chung and M. Kurisawa, *Biomaterials*, 2010, **31**, 8608-8616.
105 43. L. S. Wang, P. Y. Chow, T. T. Phan, I. J. Lim and Y. Y. Yang, *Advanced Functional Materials*, 2006, **16**, 1171-1178.
44. B. G. Kabra, S. H. Gehrke and R. J. Spontak, *Macromolecules*, 1998, **31**, 2166-2173.
45. V. Karageorgiou and D. Kaplan, *Biomaterials*, 2005, **26**, 5474-5491.
110 46. J. Ma, C. Wang and K. W. Peng, *Biomaterials*, 2003, **24**, 3505-3510.
47. R. M. Pilliar, M. J. Filiaggi, J. D. Wells, M. D. Grynpas and R. A. Kandel, *Biomaterials*, 2001, **22**, 963-972.
48. E. Romero and P. Simms, *Geotech Geol Eng*, 2008, **26**, 705-727.
49. Ž. Zuzana, G. Eva and P. Willi, *Processing and Application of*
115   *Ceramics*, 2008, **2**, 1-8.

50. Q. Liu, Y. Li, S. Shen and Z. Shanshan, *Materials Chemistry and Physics*, 2011, **125**, 315-318.

51. R. van Dijkhuizen-Radersma, L. Moroni, A. v. Apeldoorn, Z. Zhang and D. Grijpma, in *Tissue Engineering*, eds. B. Clemens van, T. Peter, L. Anders, H. Jeffrey, F. W. David, C. Ranieri, D. d. B. Joost, P. T. A. L. J. H. D. F. W. R. C. J. D. d. B. Jérôme SohierA2 - Clemens van Blitterswijk and S. Jérôme, Academic Press, Burlington, 2008, pp. 193-221.

52. M. Märtson, J. Viljanto, T. Hurme, P. Laippala and P. Saukko, *Biomaterials*, 1999, **20**, 1989-1995.

53. K. S. Anseth, V. R. Shastri and R. Langer, *Nat Biotech*, 1999, **17**, 156-159.

54. L. S. Nair and C. T. Laurencin, *Progress in Polymer Science*, 2007, **32**, 762-798.

55. C. B. Hutson, J. W. Nichol, H. Aubin, H. Bae, S. Yamanlar, S. Al-Haque, S. T. Koshy and A. Khademhosseini, *Tissue engineering. Part A*, 2011, **17**, 1713-1723.

56. Q. Li, J. Wang, S. Shahani, D. D. N. Sun, B. Sharma, J. H. Elisseeff and K. W. Leong, *Biomaterials*, 2006, **27**, 1027-1034.

57. A. J. García and D. Boettiger, *Biomaterials*, 1999, **20**, 2427-2433.

58. C. Chang and L. Zhang, *Carbohydrate Polymers*, 2011, **84**, 40-53.

59. Y. Ke, Y. J. Wang, L. Ren, Q. C. Zhao and W. Huang, *Acta Biomaterialia*, 2010, **6**, 1329-1336.

60. Y. Chen and L. Liu, *Advanced drug delivery reviews*, 2012, **64**, 640-665.

61. H. Li, J. R. Friend and L. Y. Yeo, *Biomaterials*, 2007, **28**, 4098-4104.

62. A. G. Cristancho and M. A. Lazar, *Nature reviews. Molecular cell biology*, 2011, **12**, 722-734.

63. C. Yu, J. Bianco, C. Brown, L. Fuetterer, J. F. Watkins, A. Samani and L. E. Flynn, *Biomaterials*, 2013, **34**, 3290-3302.

64. K. Comley and N. A. Fleck, *International Journal of Solids and Structures*, 2010, **47**, 2982-2990.

65. D. H. Stacey, S. E. Hanson, G. Lahvis, K. A. Gutowski and K. S. Masters, *Tissue engineering. Part A*, 2009, **15**, 3389-3399.

66. F. Guilak, D. M. Cohen, B. T. Estes, J. M. Gimble, W. Liedtke and C. S. Chen, *Cell stem cell*, 2009, **5**, 17-26.

67. N. Huebsch, P. R. Arany, A. S. Mao, D. Shvartsman, O. A. Ali, S. A. Bencherif, J. Rivera-Feliciano and D. J. Mooney, *Nat Mater*, 2010, **9**, 518-526.

68. M. P. Lutolf, P. M. Gilbert and H. M. Blau, *Nature*, 2009, **462**, 433-441.

69. K. A. Kilian, B. Bugarija, B. T. Lahn and M. Mrksich, *Proceedings of the National Academy of Sciences of the United States of America*, 2010, **107**, 4872-4877.

70. R. McBeath, D. M. Pirone, C. M. Nelson, K. Bhadriraju and C. S. Chen, *Developmental Cell*, 2004, **6**, 483-495.

71. S. A. Ruiz and C. S. Chen, *Stem Cells*, 2008, **26**, 2921-2927.

Graphical Abstract
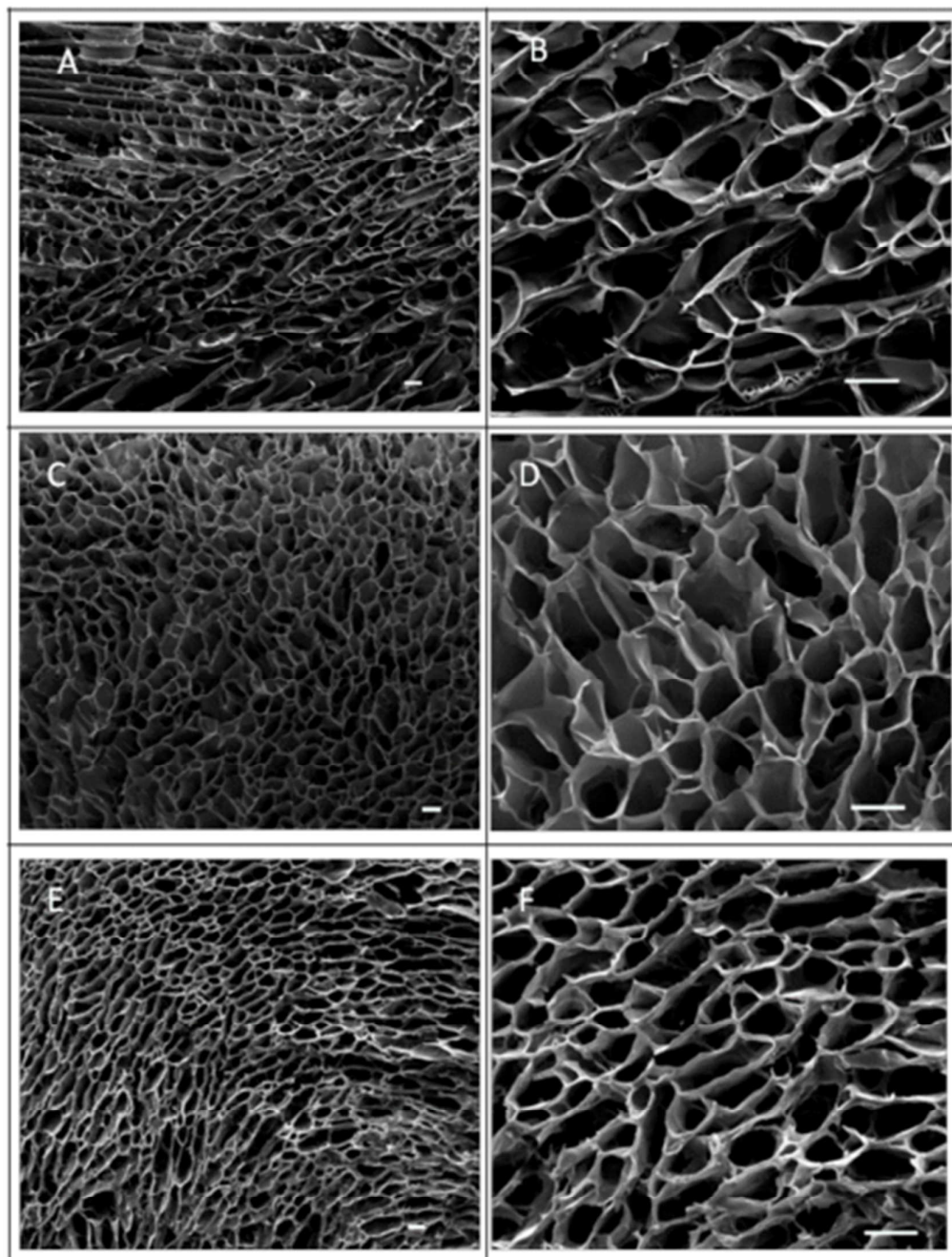
This study describes the preparation and characterization of a biodegradable and porous 3D hydrogel constructed from hydroxypropyl cellulose, modified with bifunctional hydroxpropyl cellulose methacrylate, for adipose tissue engineering applications.

Gene	5' to 3' Sequence (sense)	5' to 3' Sequence (antisense)
GAPDH	CCCCTTCATTGACCTCAACTACA	TTGCTGATGATCTTGAGGCTGT
PPARG	CTCCTATTGACCCAGAAAGC	GTAGAGCTGAGTCTTCTCAG
LPL	ATGGAGAGCAAAGCCCTGCTC	GTTAGGTCCAGCTGGATCGAG
Leptin	GTGCC-TATCCAGAAAGTCCAG	TCAGCATTCAGGGCTAACA TC
Adiponectin	CATGACCAGGAAACCACGACT	TGAATGCTGAGCGGTAT

Table 1. PCR primers
200x81mm (72 x 72 DPI)
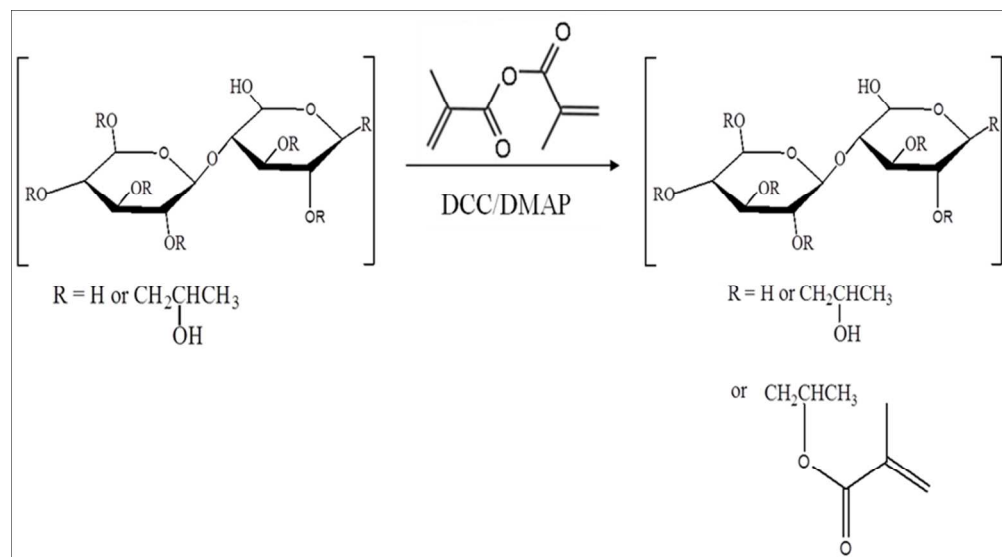
Fig. 1a Synthesis scheme of HPC-MA
256x127mm (135 x 150 DPI)
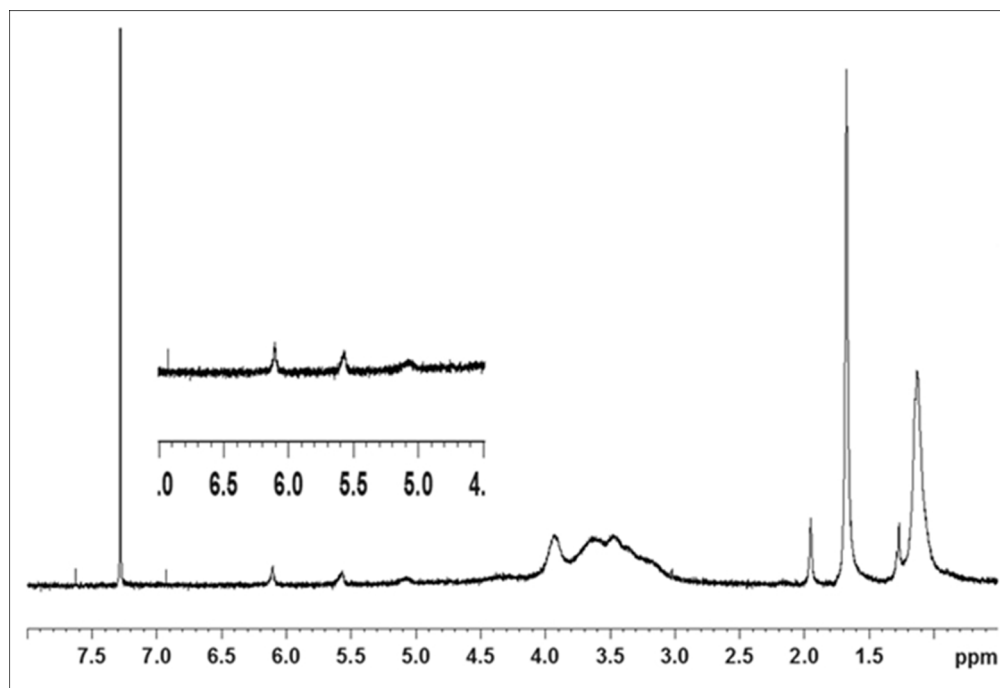
Fig. 1b NMR of HPC-MA in CDCl$_3$
164x112mm (150 x 150 DPI)
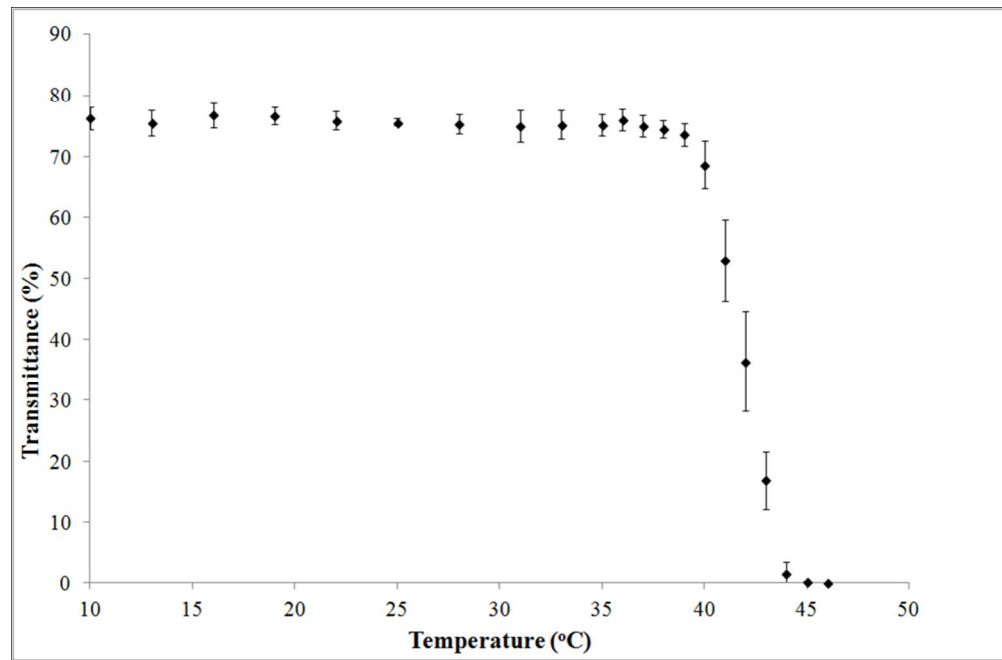
Fig. 1c Turbidimetry measurement for HPC-MA-10 %. The data are shown as mean values with standard deviation as error bars in the form of mean value ± standard deviation.
260x170mm (96 x 96 DPI)
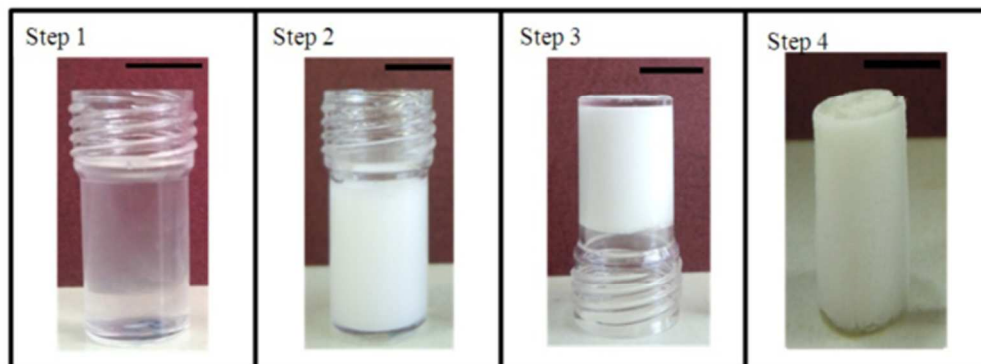
Fig. 1d Preparation of HPC-MA scaffold (scale bar 1.0 cm) from (Step 1) homogenous solution of HPC-MA-10 % at room temperature, to (Step 2) phase separated colloidal fluid at ~ 45 $^{\circ}$C, (Step 3) crosslinked heterogeneous gel at room temperature and (Step 4) freeze-dried scaffold.
222x83mm (72 x 72 DPI)
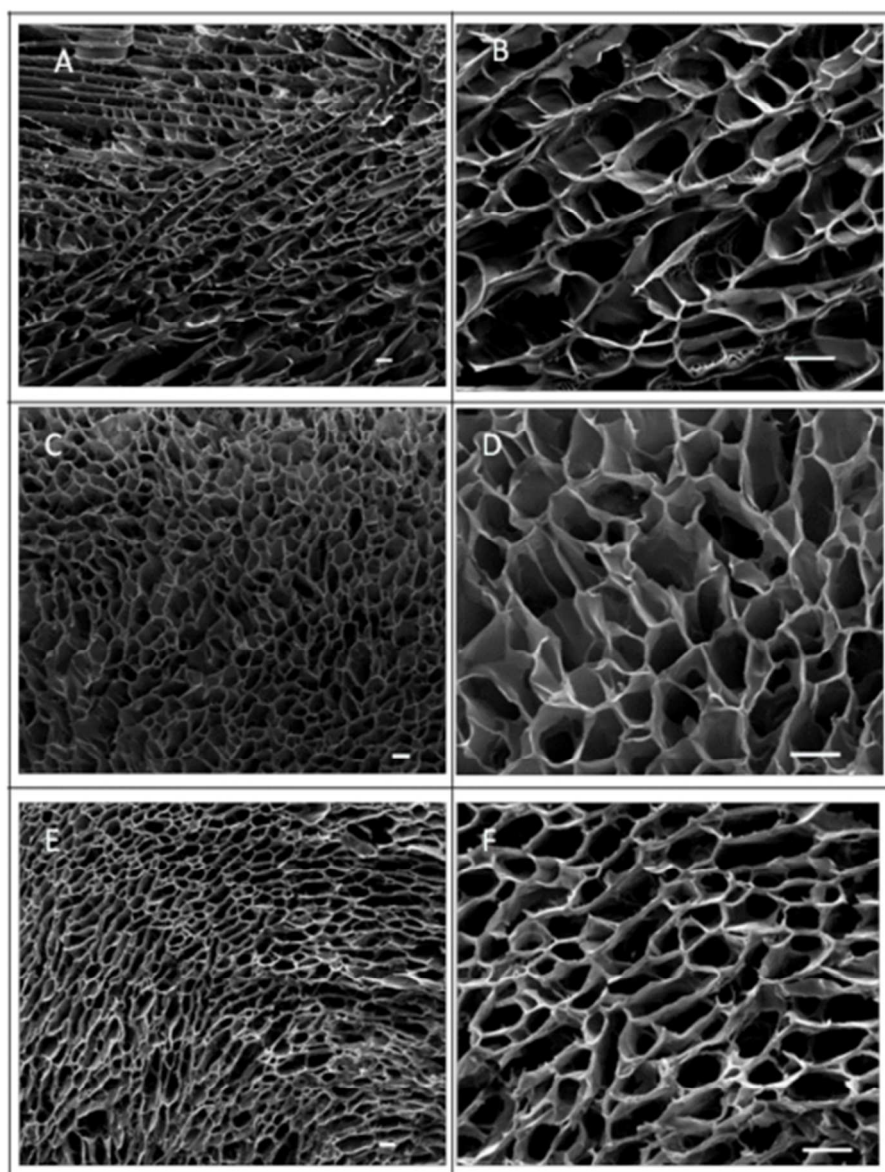
Fig. 3 Pore size and morphology of HPC-MA scaffolds. (A) and (B), (C) and (D), (E) and (F) are representative cross-sectional SEM of lyophilised HPC-MA-10 wt%, 15 wt% and 20 wt% , at low and high magnification (scale bar 100 μm), respectively.micrographs
172x225mm (72 x 72 DPI)
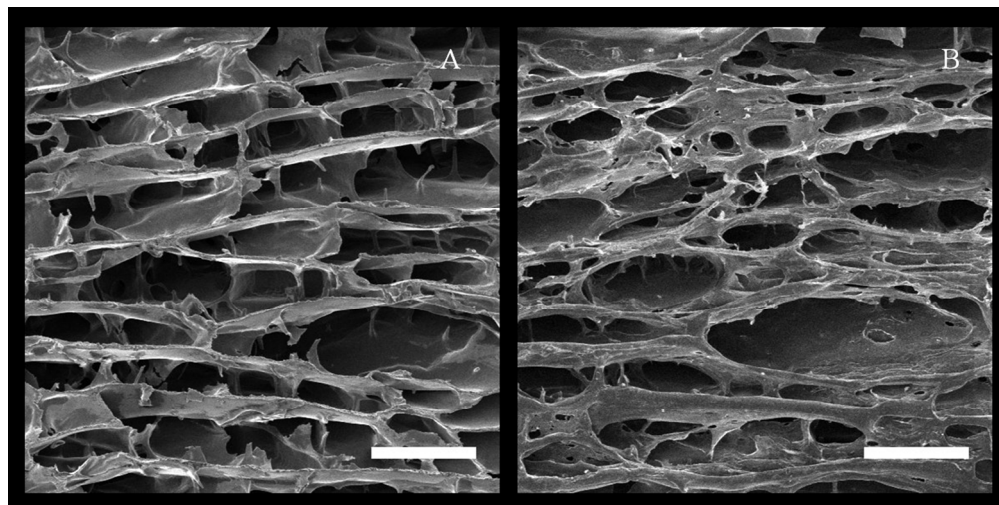
Fig. 4a FIB/SEM of HPC-MA-10 wt% (scale bar 100 μm), top view SEM image of the scaffold before milling (A), after a layer of approximately 50 μm in thickness milled off by FIB (B)
227x114mm (150 x 150 DPI)
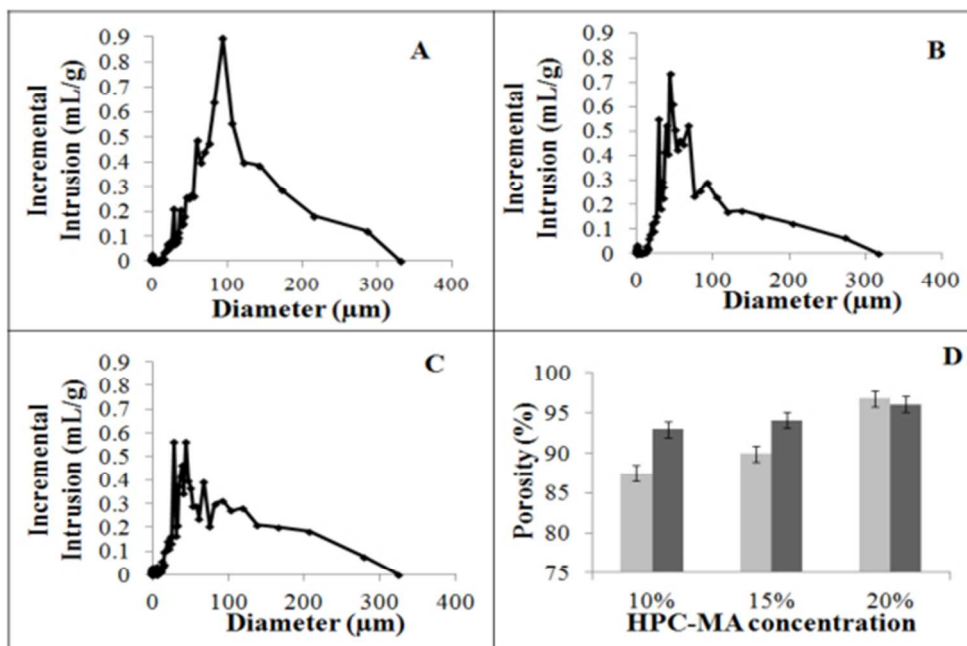
Fig. 4b Pore size distribution of HPC-MA-0.35-10 wt% (A), 15 wt% (B) and 20 wt% (C); Porosity (grey square) and interconnected porosity (black square) of HPC-MA scaffold (D). The data are shown as mean values with standard deviation as error bars in the form of mean value ± standard deviation.
210x140mm (72 x 72 DPI)
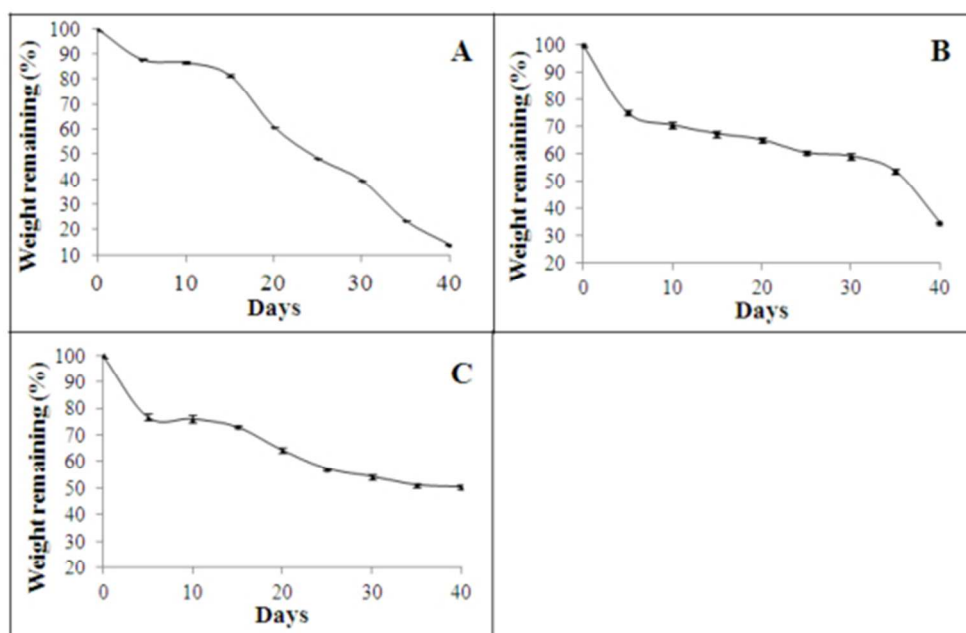
Fig. 5 Degradation profile of HPC-MA-10 wt% (A), 15 wt% (B) and 20 wt% (C). The data are shown as mean values with standard deviation as error bars in the form of mean value ± standard deviation, and the standard deviations appear to be small.

203x134mm (72 x 72 DPI)
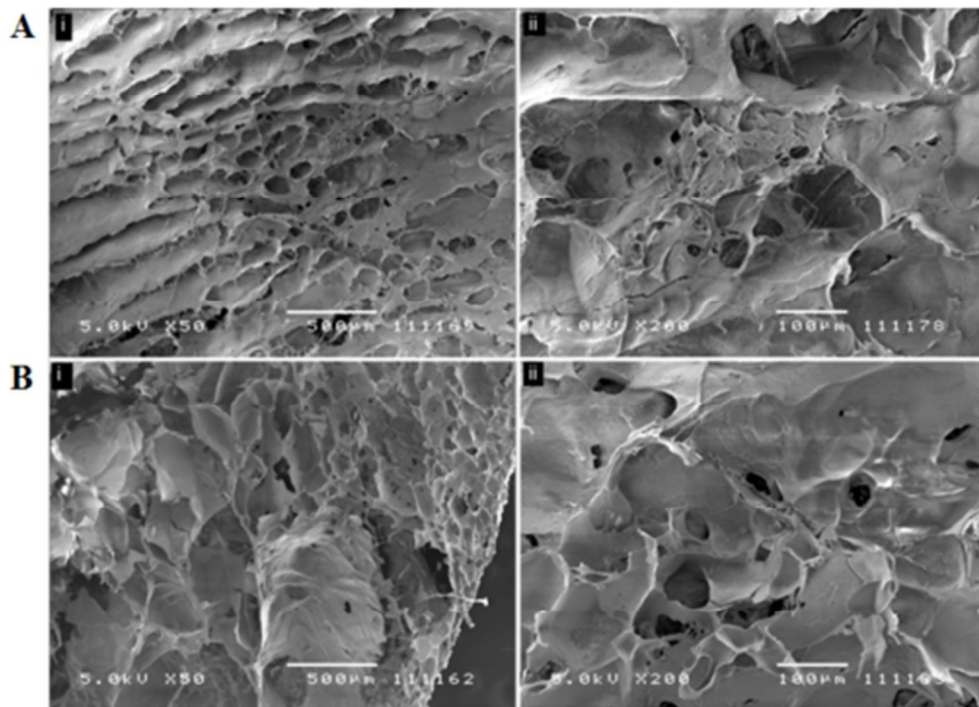
Fig. 6 SEM micrographs illustrating the presence of ASCs on the (A) 20 surface and (B) cross-section of Day 14 cell cultured HPC-MA-10 wt% scaffolds at (i) 50X and (ii) 200X magnifications.
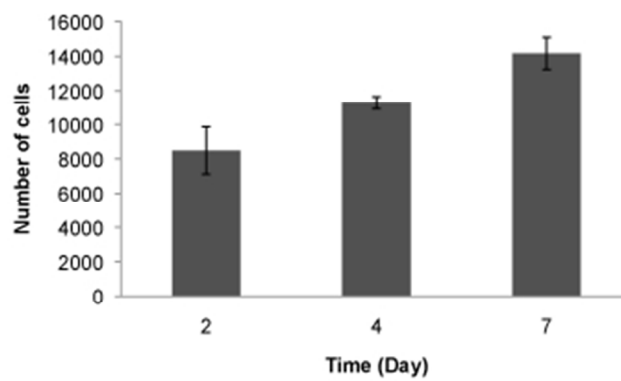
181x131mm (72 x 72 DPI)

Fig. 7 Number of ASCs in the HPC-MA-10 wt% scaffolds over a period of one week
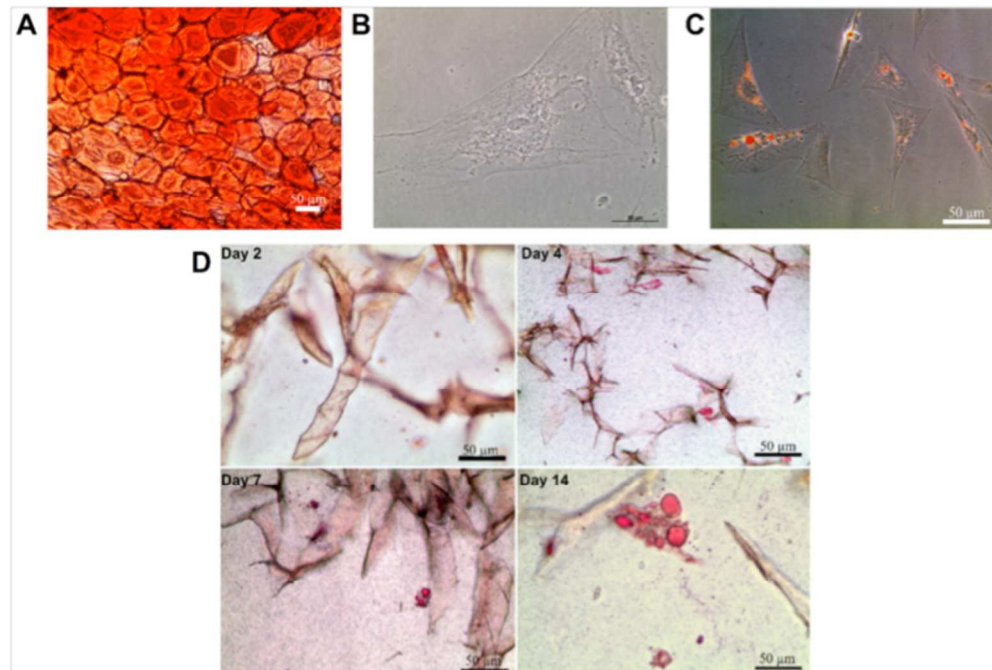190x133mm (72 x 72 DPI)

Fig. 8 Oil Red O staining of the lipid droplets of (A) fat tissue, (B) ASCs grown on 2D TCP without adipogenic supplement, (C) ASCs grown on 2D TCP with adipogenic supplment (Day 14), and (D) ASCs grown in the 3D HPC-MA-10 wt% scaffold over a period of 14 days and lipid droplets were observed to be present from Day 4 onwards. Scale bar 50μm
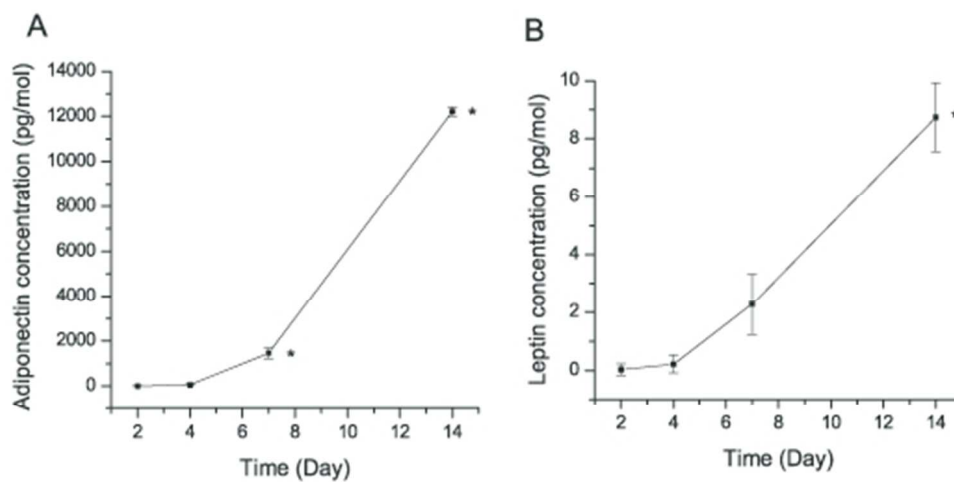
266x178mm (72 x 72 DPI)

Fig. 9 Amount of (A) adiponectin and (B) leptin released into the medium over a period of 14 days. Both adiponectin and leptin were released from Day 4 onwards, and the amount released increased significantly after 14 days of culture (*$p < 0.05$, n=3). The data are shown as mean values with standard deviation as error bars in the form of mean value ± standard 5 deviation, and the standard deviations appear to be small.
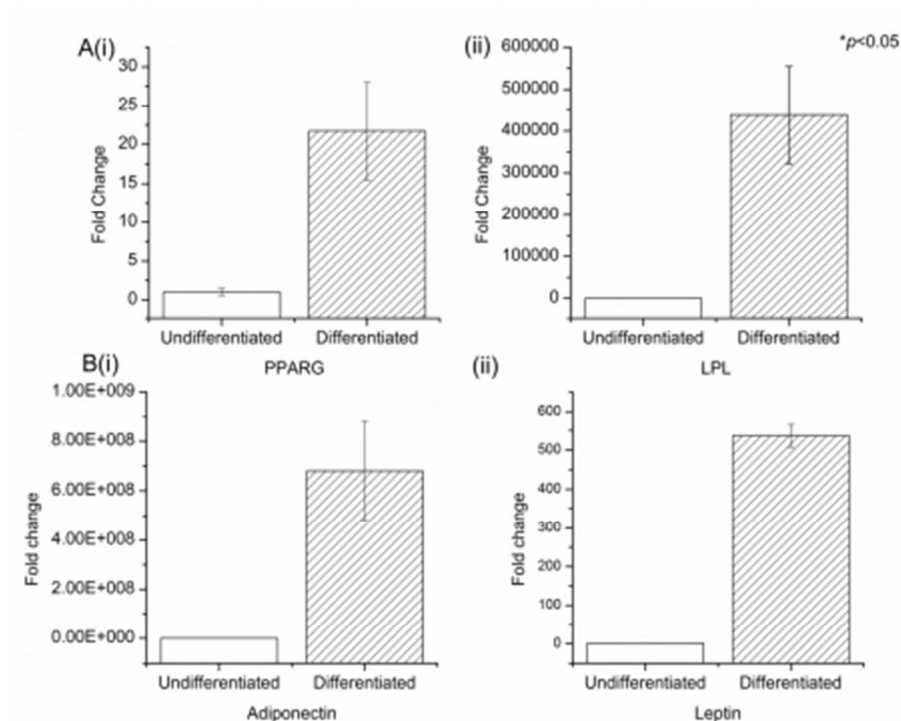190x100mm (72 x 72 DPI)

Fig. 10 PCR results for ASCs cultured in the scaffolds with adipogenic supplements compared to undifferentiated ASCs (control). Fold change values of the samples were shown for (A) early adipogenic markers (i) PPARG and (ii) LPL, and (B) late adipogenic markers (i) adiponectin and (ii) leptin. The upregulation of adipogenic markers suggests that the 3D microenvironment together with the adipogenic supplements led to the 40 differentiation of ASCs into adipocytes (*p<0.05, n=3).
161x127mm (72 x 72 DPI)